Inorganic Chemistry

Article

pubs.acs.org/IC

Photocatalytic Hydrogen Production over Chromium Doped Layered Perovskite Sr_2TiO_4

Xiaoqin Sun,[†] Yinghao Xie,[†] Fangfang Wu,[†] Hongmei Chen,[†] Meilin Lv,[†] Shuang Ni,[‡] Gang Liu,[§] and Xiaoxiang Xu*[,†]

[†]Shanghai Key Lab of Chemical Assessment and Sustainability, Department of Chemistry, Tongji University, 1239 Siping Road, Shanghai, 200092, China

[‡]Science and Technology on Plasma Physics Laboratory, Laser Fusion Research Center, China Academy of Engineering Physics, Mianyang 621900, China

[§]Shenyang National Laboratory for Materials Science, Institute of Metal Research, Chinese Academy of Science, 72 Wenhua Road, Shenyang 110016, China

ABSTRACT: Layered semiconductor photocatalysts have been found to exhibit promising performance levels, probably linked to their interlayer framework that facilitates separation of charge carriers and the reduction/oxidation reactions. Layered titanates, however, generally demonstrate activities under UV irradiation, and therein lies the strong desire to extend their activity into the visible light region. Here, we investigated a series of layered perovskite by doping Sr_2TiO_4 with Cr and/or La in the hope to improve their visible light responses. Their crystal structures and other physicochemical properties were systematically explored. Our results show that La and Cr can be successfully accommodated in the layered structure and Cr is an efficient dopant for the extension of visible light absorbance. Much enhanced photocatalytic hydrogen evolution was observed after doping and was found to be composition-dependent. The highest hydrogen production rate approaches 97.7 μmol/h for $Sr_2Ti_{0.95}Cr_{0.05}O_{4-\delta}$ under full range irradiation ($\lambda \geq 250$ nm) and 17 μmol/h for $Sr_2Ti_{0.9}Cr_{0.1}O_{4-\delta}$ under visible light irradiation ($\lambda \geq 400$ nm), corresponding to an apparent quantum efficiency of 0.16% and 0.05%, respectively. Theoretical calculation reveals that the improved optical and photocatalytic properties are owing to a newly formed spin-polarized valence band from Cr 3d orbitals. The decreased unit cell parameters, reduced band gaps as well as anisotropic properties of layered architectures are likely the reasons for a better activity. Nevertheless, instability of these compounds in the presence of moisture and CO_2 was also noticed, suggesting that protective atmospheres are needed for the storage of these photocatalysts.

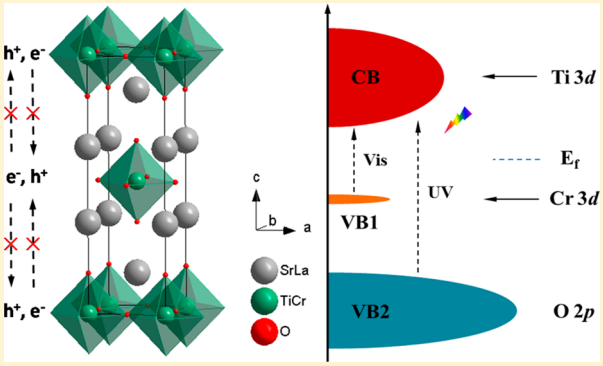

1. INTRODUCTION

Photocatalytic hydrogen production from water using a heterogeneous semiconductor has been considered as an appealing route for the establishment of a renewable energy infrastructure, not only from energy security concerns but also with environmental considerations.[1] The scalable application of this technique hinges on the fundamental improvements on photocatalytic materials, which, by far, lies in the development of visible light active semiconductors. Most of the semiconductors investigated previously have their intrinsic band gaps too large to utilize visible light photons and, therefore, are subject to low solar energy conversion efficiency.[2] One of the most efficient means of modifying a wide band gap semiconductor is doping, which involves the introduction of foreign atoms into the crystal structures of native semiconductors.[3] Owing to the formation of additional bands/energy levels within their intrinsic band gaps, doping could significantly reduce the threshold for the light absorbance. A typical example is $SrTiO_3$, which has a band gap of about 3.2 eV. By doping with a wealth of elements such as Cr,[4] Ni,[5] Fe,[6] Mn,[7] and Rh,[8] or codoping with several elements such as Cr/Ta,[4a] Ni/Nb,[5] Rh/Sb,[9] La/Cr,[10] La/Rh,[11] La/Ni,[12] etc., $SrTiO_3$ is capable of absorbing visible light photons and demonstrates interesting photocatalytic activity. A recent study shows that Cr seems to be the best dopant for $SrTiO_3$ among various elements and codoping with La is beneficial for the suppression of detrimental Cr^{6+} species.[10] On the other hand, layered materials often exhibit interesting photocatalytic properties and are attracting most attention.[13] Layered titanates and niobates, in particular, have shown promising performance under UV irradiation that complete water splitting into H_2 and O_2 is achieved.[14] It is, therefore, of great interest to modify these layered materials with doping techniques for the improvement of their visible light activity. Here, we carried out a systematic study on the doping of layered perovskite material Sr_2TiO_4 with

Received: May 12, 2015
Published: July 14, 2015

DOI: 10.1021/acs.inorgchem.5b01042
Inorg. Chem. 2015, 54, 7445−7453

Cr in terms of crystal structure, stability, and photocatalytic properties. Sr_2TiO_4 is one of the end materials in the Ruddlesden–Popper series $Sr_{n+1}Ti_nO_{3n+1}$ ($n \geq 1$) and is layering parallel to $\{001\}_p$.[15] It has the highest amounts of interlayers among the entire series that each layer of the TiO_6 octahedron is separated by two layers of SrO. More importantly, recent investigations on the surface of perovskite type materials indicated that the perovskite surface is essentially of relevant Ruddlesden–Popper series structures.[16] The formation of layered materials on the surface of perovskite compounds shall have profound influence on the photocatalytic performance as all photocatalytic reactions proceed at the surface.[17] It is, therefore, of critical importance to closely examine the layered Ruddlesden–Popper series compound Sr_2TiO_4 for a better understanding of perovskite photocatalysts.

2. EXPERIMENTAL SECTION

2.1. Material Synthesis. Materials were prepared by conventional solid-state reactions. Cr doped and La/Cr codoped samples were prepared for comparisons. The doping level was controlled as 5 mol % and 10 mol %, i.e., $Sr_2Ti_{0.95}Cr_{0.05}O_{4-\delta}$, $Sr_2Ti_{0.9}Cr_{0.1}O_{4-\delta}$, $Sr_{1.95}La_{0.05}Ti_{0.95}Cr_{0.05}O_4$, and $Sr_{1.9}La_{0.1}Ti_{0.9}Cr_{0.1}O_4$. Pristine Sr_2TiO_4 was also synthesized for comparisons. Starting materials are $SrCO_3$ (Aladdin, 99.9%), La_2O_3 (Aladdin, 99.9%), TiO_2 (Aladdin, 99.9%), and Cr_2O_3 (Aladdin, 99.9%). The powders were subjected to a thermal treatment at 300 °C for 5 h prior to weighing in order to remove moisture absorbed. In a typical synthesis of $Sr_{1.9}La_{0.1}Ti_{0.9}Cr_{0.1}O_4$, 2.8078 g of $SrCO_3$, 0.1629 g of La_2O_3, 0.7220 g of TiO_2, and 0.0761 g of Cr_2O_3 were thoroughly mixed using an agate mortar and pestle. The finely blended mixtures were then uniaxially pressed into pellets under a pressure of 5 tons. The resulting pellets were transferred into alumina crucibles and calcined in a muffle furnace at 1573 K for 40 h. Intermediate grindings and recalcination were applied in order to remove any impurity present. The calcined pellets were then ground into powders and were collected for further experiments.

2.2. Method. Phase purity and crystal structure were examined by using X-ray powder diffraction (XRD) techniques (Bruker D8 Focus diffractometer). Incident radiation used were Cu Kα_1 (λ = 1.5406 Å) and Cu Kα_2 (λ = 1.5444 Å). The step size for data collection was 0.01° with a collection time of 100 s for each step. The General Structure Analysis System (GSAS) software package was applied to perform Rietveld refinement.[18] Microstructures of prepared samples were analyzed by a field emission scanning electron microscope (Hitachi S4800). Chemical compositions and binding energy of individual elements were analyzed using X-ray photoelectron spectroscopy (Thermo Escalab 250 with a monochromatic Al Kα X-ray source). All binding energies were referenced to the C 1s peak at 284.7 eV from adventitious carbon.[19] Optical absorption spectra were collected and analyzed using a UV–vis spectrophotometer (JASCO-V750) and the JASCO software suite, and the reference nonabsorbing material is $BaSO_4$.[20]

2.3. Photocatalytic Activity. Photocatalytic activity of as-prepared samples was evaluated in a top-irradiation-type reactor connected to a gas-closed circulation and evacuation system (Perfect Light, Labsolar-IIIAG). In a typical experiment, 0.1 g of the sample powders was dispersed in 100 mL of aqueous solution and these samples were sealed in the reactor. Na_2SO_3 (0.05 M) was used as a sacrificial agent, and Pt (1 wt %) was applied as a cocatalyst. The loading of Pt onto the sample powders was performed by a thermal deposition method:[21] proper amounts of H_2PtCl_6 aqueous solution were impregnated into sample powders, and these were heated on a hot plate at 90 °C until dry. Thereafter, the temperature was raised to 180 °C for 2 h to fully decompose H_2PtCl_6 into Pt nanoparticles. A 500 W high-pressure mercury lamp (NBeT, Merc-500) was used as a light source, which is coupled with a UV cutoff filter ($\lambda \geq 400$ nm) to generate visible light irradiation. The photon flux of the lamp is calibrated using a quantum meter (Apogee MP-300). The recorded photon flux is ~1543.9 μmol/m^2/s for full range irradiation ($\lambda \geq 250$ nm) and ~796.5 μmol/m^2/s for visible light irradiation ($\lambda \geq 400$ nm). A water jacket was used to stabilize the reactor temperature around 20 °C. The gas component within the reactor was then analyzed using an on-line gas chromatograph (TECHCOMP, GC7900) with a TCD detector (5 Å molecular sieve columns and Ar carrier). The apparent quantum efficiency is then calculated using the following equation:

$$\text{Apparent quantum efficiency} = 2 \times \text{moles of hydrogen production per hour/moles of photon flux per hour} \times 100\%$$

2.4. Theoretical Calculations. Theoretical calculations were performed using the density functional theory (DFT) implemented in the Vienna Ab initio Simulation Package (VASP).[22] The Perdew, Burke, and Ernzerhof (PBE) exchange-correlation functional within the generalized gradient approximation (GGA)[23] and the projector augmented-wave pseudopotential were applied.[24] Spin-polarization was also considered in samples containing Cr during calculation. A unit cell ($a = b$ = 3.88 Å, c = 12.60 Å, $\alpha = \beta = \gamma = 90°$) with tetragonal symmetry was constructed for Sr_2TiO_4 simulations (total atom number =14). A 2 × 2 × 1 super cell ($a = b$ = 7.77 Å, c = 12.60 Å, $\alpha = \beta = \gamma = 90°$) was constructed for simulations of the La/Cr codoped or solely Cr doped sample (total atom number = 56). The doping was considered by assuming that 1 Sr atom and 1 Ti atom were substituted by 1 La atom and 1 Cr atom in the La/Cr codoped sample and 1 Ti atom was substituted by 1 Cr atom in the solely Cr doped one, respectively. All geometry structures were fully relaxed until the forces on each atom are less than 0.01 eV/Å. Static calculations were done with a 13 × 13 × 4 Monkhorst–Pack k-point grid for Sr_2TiO_4 simulations and a 4 × 4 × 3 Monkhorst–Pack k-point grid for doped samples, respectively.[25]

3. RESULTS AND DISCUSSION

3.1. Phase Composition and Crystal Structure. X-ray powder diffraction patterns of freshly prepared samples are displayed in Figure 1. All samples show similar patterns that can

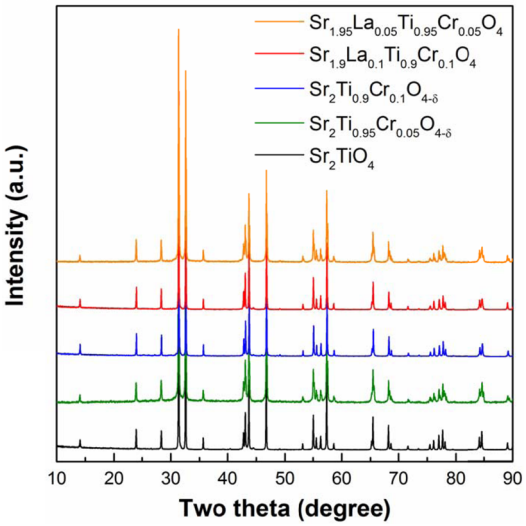

Figure 1. X-ray powder diffraction patterns of freshly prepared samples.

be indexed with a tetragonal symmetry, confirming the formation of a single phase. La and Cr cations were, therefore, successfully accommodated into the crystal structure of Sr_2TiO_4, probably in a similar manner to perovskite material $SrTiO_3$. Rietveld refinement of XRD patterns suggested that the layered structure is maintained with space group $I4/mmm$

DOI: 10.1021/acs.inorgchem.5b01042
Inorg. Chem. 2015, 54, 7445–7453

(No. 139) and substitution between Sr and La, Ti and Cr is random. This is likely due to the similar ionic radius of these cations that perturbation to the crystal structure after doping is small.[26] The layered structure can be envisaged as the incorporation of an additional layer of SrO into the primitive $SrTiO_3$ perovskite structure that disconnects the neighboring TiO_6 octahedron along the [001] direction (Figure 2, inserted image). The refined unit cell parameters are listed in Table 1. A slight decrease of unit cell parameters was noticed after doping, probably due to the formation of Cr^{6+} species and/or oxygen vacancies when Cr is the only dopant and smaller La^{3+} cations compared with Sr^{2+} in the case of La/Cr codoping if Vegard's law strictly holds. The smallest unit cell parameters are found with sample $Sr_2Ti_{0.9}Cr_{0.1}O_{4-\delta}$.

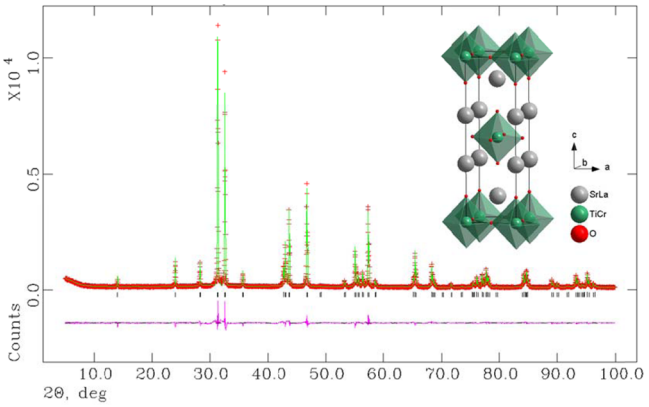

Figure 2. Observed and calculated X-ray powder diffraction patterns of $Sr_{1.95}La_{0.05}Ti_{0.95}Cr_{0.05}O_4$. The refinements converged with good *R*-factors and χ^2 (R_p = 8.82%, R_{wp} = 6.65%, χ^2 = 1.919); the refined crystal structure is shown in the inserted image.

3.2. UV–vis Spectra. The appearance of the freshly prepared samples is white for undoped Sr_2TiO_4, yellow for the La/Cr codoped sample, and violet for the Cr doped ones (Figure 3b, inserted image). The strong color of doped samples is indicative of substantial visible light absorbance. This is confirmed by their UV–vis diffuse reflectance spectra (Figure 3). Undoped Sr_2TiO_4 demonstrates a sharp absorption edge that lies within the UV region and has a band gap of around 3.5 eV, revealing its wide band gap nature. The doped samples, however, display intense absorption curves in the visible light region. In the case of the La/Cr codoped sample, two broad absorption bands can be identified, from 360 to 550 nm and from 570 to 700 nm. These two absorption bands have also been observed in La/Cr codoped $SrTiO_3$ and are attributed to $Cr^{3+} \rightarrow Ti^{4+}$ charge transfer and d–d absorption ($^4A_2 \rightarrow {}^4T_2$),[4a,b] respectively. The formal one is responsible for the visible light photocatalytic activity according to previous reports.[4a] On the contrary, Cr doped samples demonstrate an additional strong absorption band around 550 nm, which is clear evidence for the formation of Cr^{6+} species.[4a,27] Therefore, the huge color differences among doped samples are ascribed to the presence or absence of Cr^{6+} species (Figure 3b, inserted image). La obviously has an efficient annihilation function for Cr^{6+} species, likely due to a charge compensation effect.[10a] The band gap of the La/Cr codoped sample is determined to be 2.0 eV for $Sr_{1.95}La_{0.05}Ti_{0.95}Cr_{0.05}O_4$ and 1.89 eV for $Sr_{1.9}La_{0.1}Ti_{0.9}Cr_{0.1}O_4$ according to Kubelka–Munk transformation (Figure 3b). For Cr doped ones, $Cr^{3+} \rightarrow Ti^{4+}$ charge transfer is severely masked by strong d–d absorption; therefore, band gap determination is not possible.

3.3. Microstructure and Stability. Chemical stability is an important factor for the evaluation of a photocatalyst. The high Sr content in these samples implies that they may undergo phase segregation and could be vulnerable to moisture and CO_2. Here, we carried out a simple experiment by exposing the freshly prepared samples to air for the evaluation of their stability in the presence of moisture and carbon dioxide. After a period of 2 months, the powders were checked with SEM and XRD, and the results are shown in Figures 4 and 5. Under SEM conditions, all samples show large particles as large as several microns (Figure 4). Apart from the presence of these large particles, small island-like particles can be clearly identified at the surface, especially compared with the freshly prepared one (Figure 4f). XRD confirms the existence of $SrCO_3$ species according to the additional peaks around 25°. However, CO_2 attacking events seem to occur much easier in samples with higher Cr levels and the presence of La seems helpful for the alleviation of CO_2 attacking (Figure 5). The instability might originate from the lower coordination number of Sr in Sr_2TiO_4 (CN = 9), compared with stable perovskite $SrTiO_3$ (CN = 12). In light of the above observations, we conclude that layered compound Sr_2TiO_4 is not stable in the presence of CO_2 and shall be kept in a protective atmosphere. Nevertheless, the color of the sample powders remains the same.

3.4. X-ray Photoelectron Spectroscopy and Surface Compositions. The surface nature of samples after air exposure was also investigated by XPS analysis. Binding energy of core-level electrons for O, C, Ti, and Cr is shown in Figure 6 and is referenced to the C 1s peak at 284.7 eV from adventitious carbon.[19] Overlapping peaks were unfolded by fitting with different Gaussian functions. The O 1s state of all samples contains a strong peak and a shallow shoulder. The peak around 531 eV is a characteristic signal of $SrCO_3$,[28] confirming the segregation of Sr and is consistent with the observation of SEM and XRD analysis. The shallow shoulder around 529 eV can be attributed to the lattice oxygen anions 1s state.[28a] However, this peak is almost indiscernible in the case of $Sr_2Ti_{0.9}Cr_{0.1}O_{4-\delta}$, suggesting a substantial coverage of $SrCO_3$ at its surface (Figure 6a). The C 1s peaks, on the other hand, also display an extra peak around 288.6 eV along with the adventitious carbon 1s peak at 284.7 eV, which is another evidence for the formation of $SrCO_3$.[28a] Additionally, the

Table 1. Space Group and Unit Cell Parameters for Freshly Prepared Samples (Standard Deviation in Parentheses)

sample	space group	*a*/Å	*c*/Å	*V*/Å^3
Sr_2TiO_4	*I*4/*mmm*	3.8852(1)	12.5924(1)	190.083(2)
$Sr_2Ti_{0.95}Cr_{0.05}O_{4-\delta}$	*I*4/*mmm*	3.8814(1)	12.5823(1)	189.565(2)
$Sr_2Ti_{0.9}Cr_{0.1}O_{4-\delta}$	*I*4/*mmm*	3.8810(1)	12.5830(3)	189.536(10)
$Sr_{1.9}La_{0.1}Ti_{0.9}Cr_{0.1}O_4$	*I*4/*mmm*	3.8807(1)	12.5938(1)	189.669(2)
$Sr_{1.95}La_{0.05}Ti_{0.95}Cr_{0.05}O_4$	*I*4/*mmm*	3.8826(1)	12.5923(1)	189.832(5)

DOI: 10.1021/acs.inorgchem.5b01042
Inorg. Chem. 2015, 54, 7445–7453

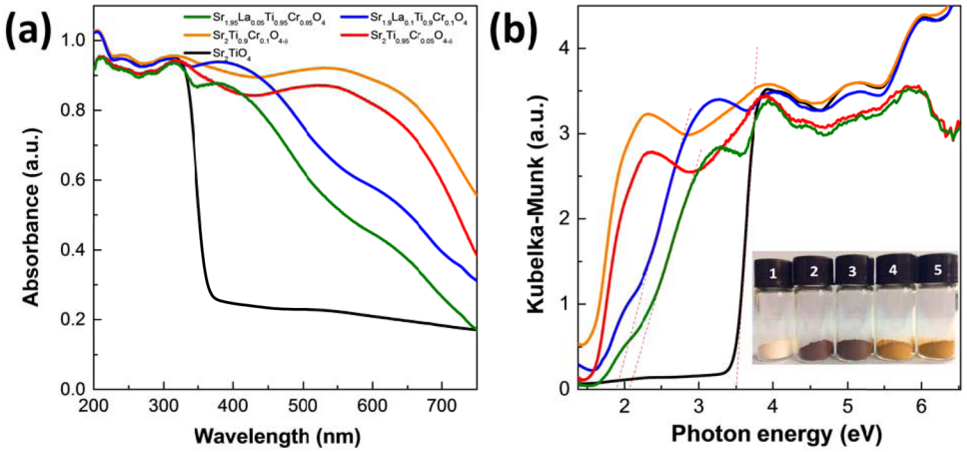

Figure 3. (a) UV−visible light absorption spectra (converted from diffuse reflectance spectra) of freshly prepared samples and (b) Kubelka−Munk transformation of diffuse reflectance data; photograph of sample powders is inserted: (1) Sr_2TiO_4, (2) $Sr_2Ti_{0.95}Cr_{0.05}O_{4-\delta}$, (3) $Sr_2Ti_{0.9}Cr_{0.1}O_{4-\delta}$, (4) $Sr_{1.9}La_{0.1}Ti_{0.9}Cr_{0.1}O_4$, (5) $Sr_{1.95}La_{0.05}Ti_{0.95}Cr_{0.05}O_4$.

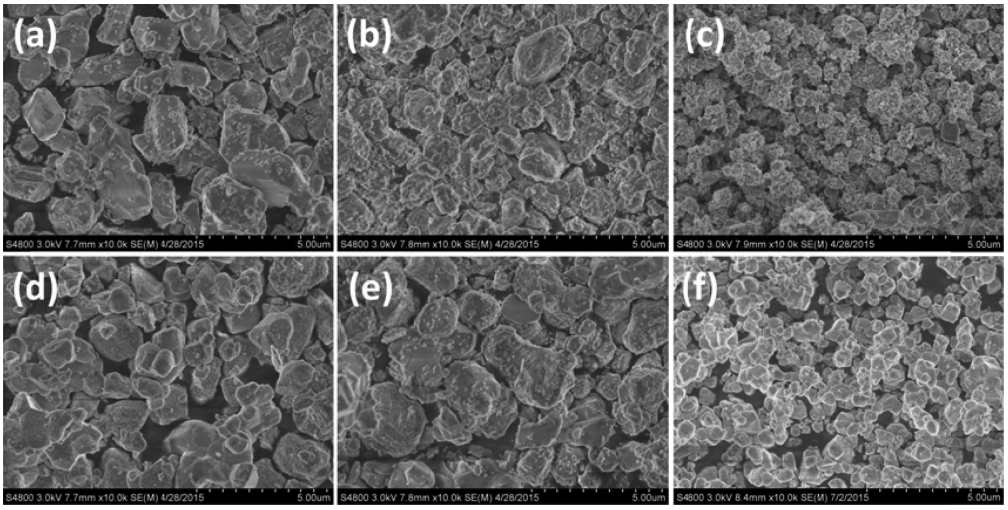

Figure 4. Field emission scanning electron microscopy images of samples exposed in air for 2 months: (a) $Sr_2Ti_{0.95}Cr_{0.05}O_{4-\delta}$, (b) $Sr_2Ti_{0.9}Cr_{0.1}O_{4-\delta}$, (c) Sr_2TiO_4, (d) $Sr_{1.95}La_{0.05}Ti_{0.95}Cr_{0.05}O_4$, (e) $Sr_{1.9}La_{0.1}Ti_{0.9}Cr_{0.1}O_4$, and (f) freshly prepared Sr_2TiO_4.

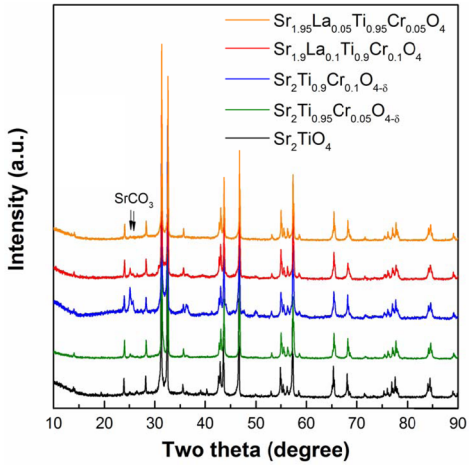

Figure 5. X-ray powder diffraction patterns of samples exposed in air for 2 months.

presence of $SrCO_3$ at the surface is accompanied by a corresponding decrease of Ti 2p signals (Figure 6c) and can be explained by the detection limit of XPS techniques in that signal collection was severely quenched by surface impurities.[19] However, the very weak signals of Cr 2p suggest that there is a strong depletion of Cr species at the surface (Figure 6d). This is also supported in the surface composition analysis in Table 2. It can be seen from the table that appreciable deviation of La, Ti, and Cr content from their stoichiometry occurs, which can only be partially explained by the formation of $SrCO_3$. The small O/Sr ratio (~2.3) implies that the surface of these layered compounds probably contains a high level of SrO species.[16a]

3.5. Photocatalytic Hydrogen Production. The photocatalytic hydrogen production was performed using sodium sulfite as a sacrificial element and Pt as a cocatalyst. A control experiment was carried out first in the dark conditions with the purpose of evaluating any reaction that does not proceed photocatalytically. No H_2 was detected in the absence of radiation, therefore, precluding any reactions that will give rise to H_2 evolution. The photocatalytic hydrogen production under full range irradiation (UV + visible light) is shown in Figure 7a. All doped samples exhibited an improved photocatalytic activity compared with undoped Sr_2TiO_4, suggesting the positive effect of introducing Cr. The highest activity was found in sample $Sr_2Ti_{0.95}Cr_{0.05}O_{4-\delta}$, where more than 320 μmol

DOI: 10.1021/acs.inorgchem.5b01042
Inorg. Chem. 2015, 54, 7445−7453

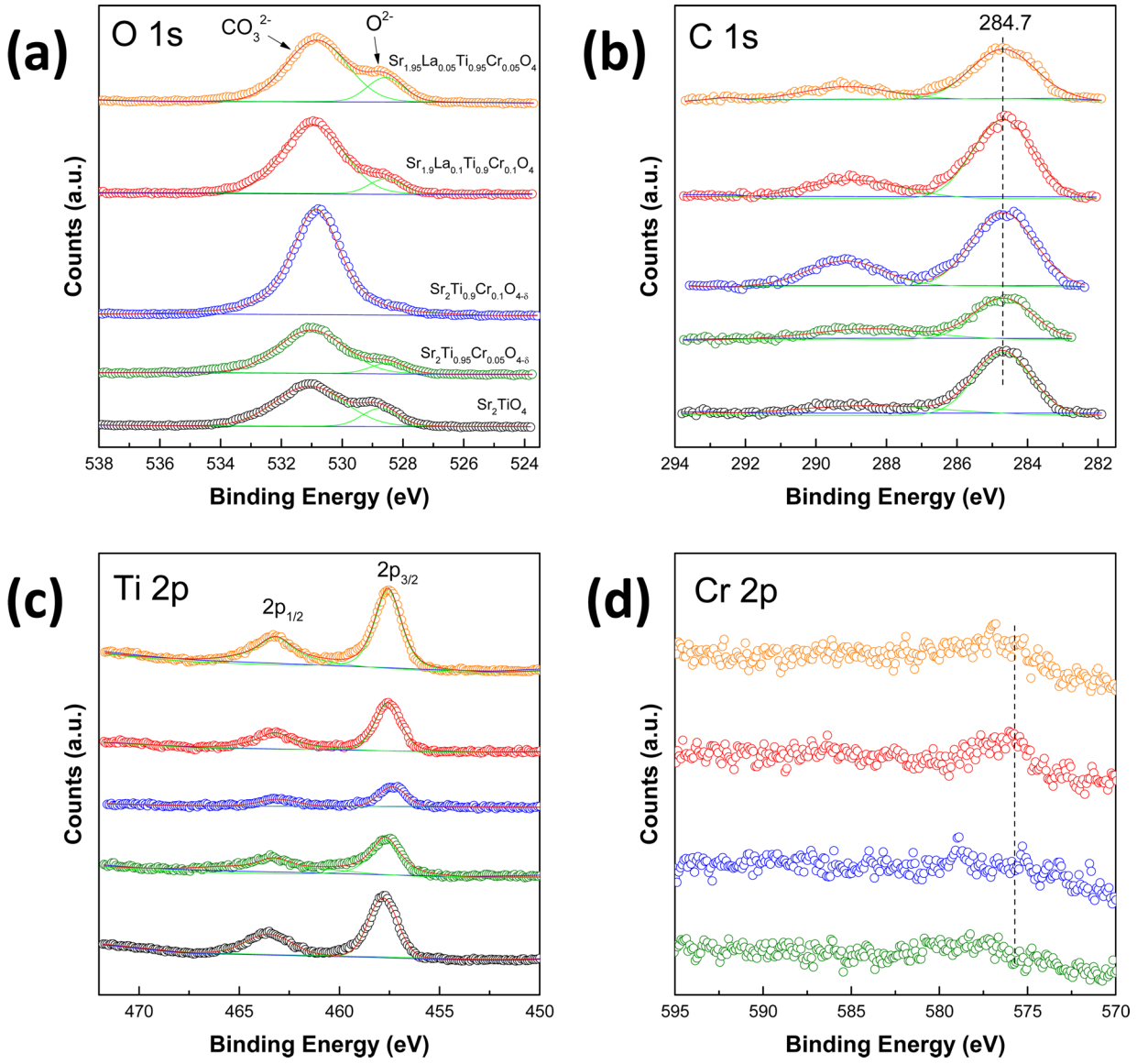

Figure 6. XPS spectra of samples exposed in air for 2 months: (a) O 1s peaks, (b) C 1s peaks, (c) Ti 2p peaks, and (d) Cr 2p peaks.

Table 2. Surface Atomic Compositions Analyzed by XPS for Samples Exposed in Air for 2 Months

sample	Sr/mol %	La/mol %	Ti/mol %	Cr/mol %	O/mol %
Sr_2TiO_4	27.17		6.74		66.09
$Sr_2Ti_{0.95}Cr_{0.05}O_{4-\delta}$	29.56		4.90	0.60	64.94
$Sr_2Ti_{0.9}Cr_{0.1}O_{4-\delta}$	30.65		1.33	0.33	67.70
$Sr_{1.9}La_{0.1}Ti_{0.9}Cr_{0.1}O_4$	25.89	1.54	3.67	0.52	68.39
$Sr_{1.95}La_{0.05}Ti_{0.95}Cr_{0.05}O_4$	28.30	0.66	5.78	0.70	64.56

of hydrogen was produced within 200 min, exceeding the amount of catalyst used (~174 μmol). Therefore, the hydrogen evolution reaction indeed proceeds photocatalytically. It is worth noting that the reaction occurs quite slowly for Cr doped samples at the beginning, which can be ascribed to the Cr^{6+} species that consumes photogenerated electrons in the initial period of experiment.[4a] This phenomenon is more pronounced in the experiment under visible light irradiation ($\lambda \geq 400$ nm) where a very long activation time is needed. Therefore, full range irradiation was first performed to activate samples prior to visible light irradiation. For a better comparison, the average hydrogen production rate was calculated after several hours irradiation and is plotted in Figure 7b. $Sr_2Ti_{0.95}Cr_{0.05}O_{4-\delta}$ demonstrated the highest hydrogen production rate ~ 97.7 μmol/h under full range irradiation, corresponding to an apparent quantum efficiency of 0.16%. This rate is more than 4-fold higher than that of pristine Sr_2TiO_4. The highest hydrogen production rate under visible light irradiation was found for sample $Sr_2Ti_{0.9}Cr_{0.1}O_{4-\delta}$ ~ 17 μmol/h, corresponding to an apparent quantum efficiency of 0.05%, even though its activity under full range irradiation is relatively lower. It is interesting to see that the La/Cr codoped sample exhibits a poorer activity under full range irradiation, although the presence of La has a positive effect for eliminating Cr^{6+} species. It has been realized

DOI: 10.1021/acs.inorgchem.5b01042
Inorg. Chem. 2015, 54, 7445−7453

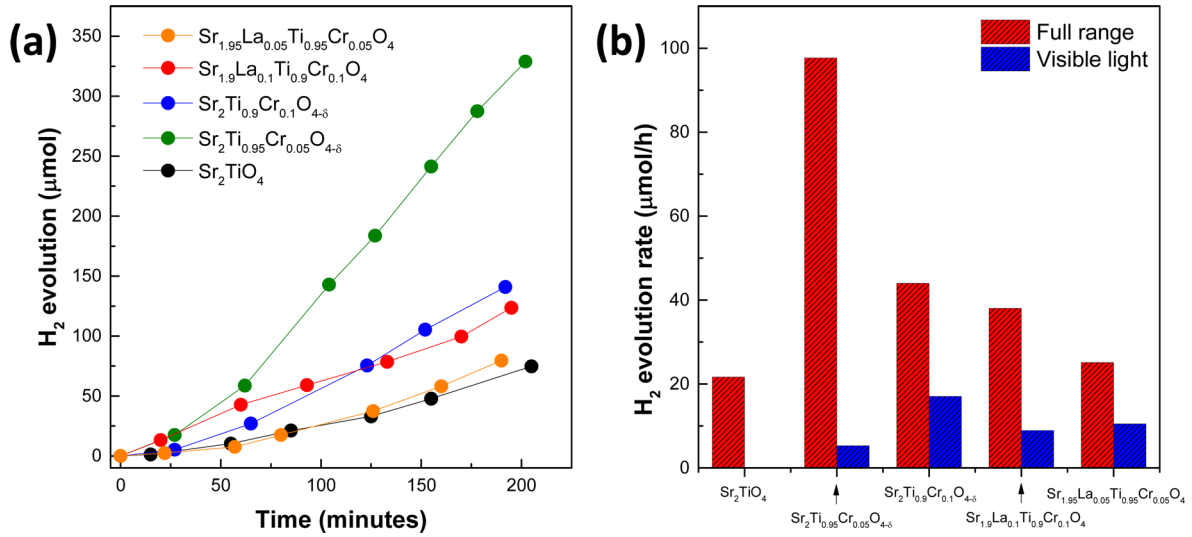

Figure 7. (a) Photocatalytic hydrogen production rate of samples under full range irradiation in sodium sulfite aqueous solution (0.05 M). (b) Plot of photocatalytic hydrogen production rate by dividing the amount of hydrogen produced with irradiation time.

that doping lower valence cations will introduce oxygen vacancies in the structure, which is beneficial for a high activity due to the inhibited formation of Ti^{3+} species.[29] Codoping La/Cr in the structure contributes to charge equilibrium so that formation of oxygen vacancies is not favored. Furthermore, a recent study on La doped $NaTaO_3$ also suggests that La will block the exposed catalytic active site; therefore, it is detrimental for photocatalytic activity.[30]

3.6. Theoretical Calculations. Theoretical calculations on the electronic structure of pristine Sr_2TiO_4 and doped ones were performed by DFT. Doping was simulated by randomly substituting Sr with La and Ti with Cr in the constructed 2 × 2 × 1 super cell ($a = b = 7.77$ Å, $c = 12.60$ Å, $\alpha = \beta = \gamma = 90°$, total atom number = 56). The calculated results are shown in Figure 8. Unlike the solely Cr doped sample, both pristine and La/Cr codoped samples are semiconductors according to the band gaps in their band structure (Figure 8). The calculated band gap for pristine Sr_2TiO_4 is 1.98 eV, which is much smaller than the experimental value of 3.5 eV from UV−vis spectra (Figure 3). This is due to the drawbacks of the generalized gradient approximation (GGA) method for underestimating band gaps.[31] Nevertheless, the calculation offers qualitative comparisons. It can be seen from the band structures that La/Cr codoped Sr_2TiO_4 has a much smaller band gap compared with Sr_2TiO_4, highlighting the positive effect of doping in improving the optical properties of Sr_2TiO_4. In the case of solely Cr doped Sr_2TiO_4, the electronic structure is generally the same as that of the La/Cr codoped one with the exception that the Fermi level lies inside the band originated from Cr 3d orbitals. Although there is a partially filled Cr 3d band, the sample remains as a semiconductor due to the highly localized nature of Cr 3d orbitals.[32] A high charge state is expected for Cr in this circumstance since less d electrons are left compared with the La/Cr codoped one, which is consistent with previous results. On the other hand, close examination of their band structures reveals the anisotropic nature of these compounds: Take the conduction band (CB) of Sr_2TiO_4, for example; the band dispersion from Γ to X controls electron behavior in the [100] direction, which covers a wide energy range ∼ 2 eV. On the contrary, negligible band dispersion can be seen from X to R, corresponding to electron behavior in the [001] direction. It is known that the effective mass of a carrier, m^*, is inversely proportional to the second derivative of the E versus k curve (wide band leads to high mobility):[33]

$$m^* = \hbar^2\left(\frac{d^2E}{dk^2}\right)^{-1}$$

Therefore, it can be inferred from the above observation that electrons will have a much higher mobility in the [100] direction than in the [001] direction. Similar trends can be found with other crystallographic directions like [110] (from Γ to M). In other words, electrons are confined in the *ab* plane and migration along the *c* axis is nearly prohibited (see Figure 2, inserted image). Since the CB of Sr_2TiO_4 is mainly composed of Ti 3d orbitals and the valence band (VB) has major contribution from O 2p orbitals (Figure 8a, PDOS), photogenerated charges are essentially circumscribed within the layered TiO_6 octahedron planes so that charge recombination between neighboring planes is effectively inhibited. The doped samples, however, all contain a new spin-polarized VB in the middle of the band gap which is primarily arising from Cr 3d orbitals. Thereby, the smaller band gap in the doped samples originated from this new VB and its visible light activity can be attributed from the excitation of electrons from this new VB to upper CB due to spin conservation law (photons have no spin), in other words, from Cr 3d orbitals to Ti 3d orbitals.

It is worth discussing the different photocatalytic activity observed among doped samples according to their band structures. Charge generation processes are schematically represented in Figure 9. Under full range irradiation (UV + visible light), both electrons from VB1 and VB2 can be excited into CB that participated in the photocatalytic reactions. The narrow VB1 formed from Cr 3d orbitals suggested that holes in this band have a poor mobility and are not as reactive as holes formed in VB2. Therefore, photocatalytic performance would be mainly controlled by the charge transfer process of $O^{2-} \rightarrow Ti^{4+}$. Small unit cell parameters (higher degree of orbital overlapping between O 2p and Ti 3d) as well as low doping level (less defects) are probably the dominating factors for a better activity under full range irradiation, as in the case of sample $Sr_2Ti_{0.95}Cr_{0.05}O_{4-\delta}$. Under visible light irradiation,

DOI: 10.1021/acs.inorgchem.5b01042
Inorg. Chem. 2015, 54, 7445−7453

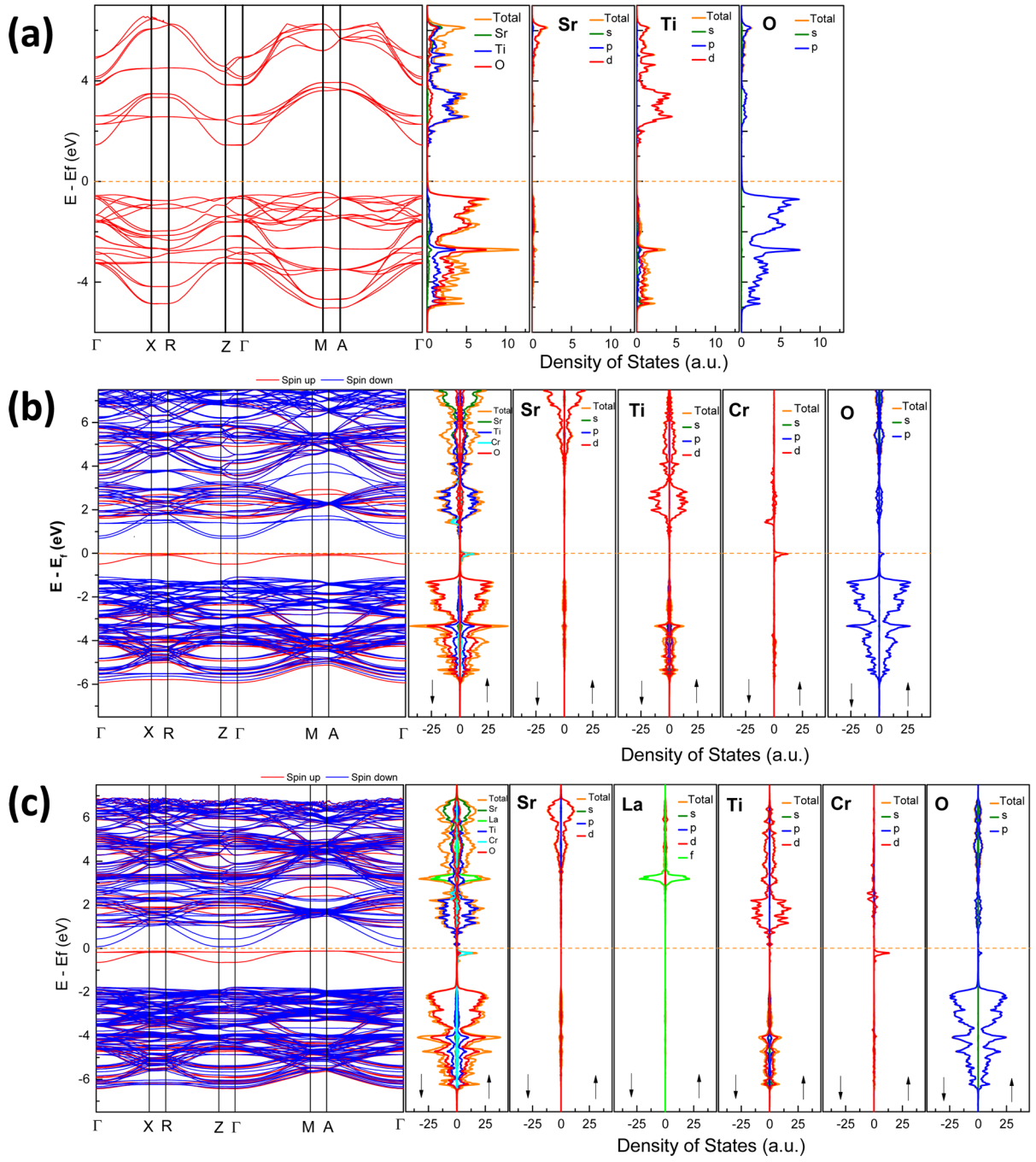

Figure 8. Calculated band structure, total density of states (DOS), and partial density of states (PDOS) of constituent elements for (a) pristine Sr_2TiO_4, (b) solely Cr doped Sr_2TiO_4, and (c) La/Cr codoped Sr_2TiO_4. Spin directions are indicated by arrows (↓↑), and the Fermi level is marked by the dotted orange lines.

however, electron excitations from VB2 to CB are prohibited; thereby, photocatalytic activity is solely attributed to the charge transfer from VB1 to CB, i.e., charge transfer process of $Cr^{3+} \rightarrow Ti^{4+}$. Apparently, a higher Cr content is beneficial for a better performance and is likely the reason why sample $Sr_2Ti_{0.9}Cr_{0.1}O_{4-\delta}$ displays a better activity.

4. CONCLUSIONS

We have investigated a series of Cr doped and La/Cr codoped layered titanates Sr_2TiO_4 in terms of crystal structure, optical properties, stability, surface states, and photocatalytic activity for hydrogen production. Our results showed that Cr and La can be successfully doped into the crystal structure of Sr_2TiO_4 with the layered architecture maintained. Introducing Cr can efficiently reduce the band gap of Sr_2TiO_4 and improve its visible light absorption. Doping Cr alone will lead to the formation of Cr^{6+} species, which could be prohibited by codoping with La. The layered Sr_2TiO_4 is essentially unstable in the presence of moisture and CO_2, probably due to the low coordination number of Sr in the structure. A strong enrichment of Sr at the surface was observed with concomitant depletion of Ti and Cr according to the XPS analysis. All doped samples showed an improved photocatalytic activity compared with undoped Sr_2TiO_4 under both full range and visible light

DOI: 10.1021/acs.inorgchem.5b01042
Inorg. Chem. 2015, 54, 7445−7453

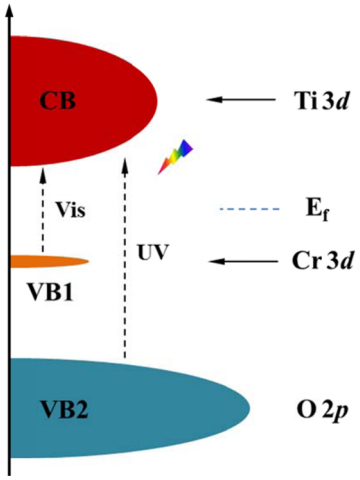

Figure 9. Schematic representation of band structures of doped samples and possible charge generation procedures; the Fermi level is marked by the dotted line.

irradiation. The best hydrogen production rate approaches 97.7 μmol/h for sample $Sr_2Ti_{0.95}Cr_{0.05}O_{4-\delta}$ under full range irradiation and 17 μmol/h for $Sr_2Ti_{0.9}Cr_{0.1}O_{4-\delta}$ under visible light irradiation, corresponding to an apparent quantum efficiency of 0.16% and 0.05%, respectively. Theoretical calculation suggests that band gap reduction after doping is due to a newly formed valence band, which is mainly composed of Cr 3d orbitals. All samples demonstrate an anisotropic property in that photogenerated charges are confined within the TiO_6 octahedron plane. The different photocatalytic behavior between full range and visible light irradiation conditions might be due to that different charge generation processes occurred.

AUTHOR INFORMATION

Corresponding Author

*E-mail: xxxu@tongji.edu.cn. Phone: +86-21-65986919.

Notes

The authors declare no competing financial interest.

ACKNOWLEDGMENTS

We thank the Young Scientists Fund of the National Natural Science Foundation of China (Grant No. 21401142) for funding and the Recruitment Program of Global Youth Experts (1000 plan). We also thank the Science & Technology Commission of Shanghai Municipality (14DZ2261100).

REFERENCES

(1) (a) Lewis, N. S.; Nocera, D. G. *Proc. Natl. Acad. Sci. U.S.A.* **2006**, *103* (43), 15729−15735. (b) Kudo, A.; Miseki, Y. *Chem. Soc. Rev.* **2009**, *38* (1), 253−278. (c) Osterloh, F. E. *Chem. Mater.* **2008**, *20* (1), 35−54.

(2) (a) Linic, S.; Christopher, P.; Ingram, D. B. *Nat. Mater.* **2011**, *10* (12), 911−921. (b) Listorti, A.; Durrant, J.; Barber, J. *Nat. Mater.* **2009**, *8* (12), 929−U22. (c) Xu, X. X.; Randorn, C.; Efstathiou, P.; Irvine, J. T. S. *Nat. Mater.* **2012**, *11* (7), 595−598.

(3) Xu, X. X.; Azad, A. K.; Irvine, J. T. S. *Catal. Today* **2013**, *199*, 22−26.

(4) (a) Ishii, T.; Kato, H.; Kudo, A. *J. Photochem. Photobiol., A* **2004**, *163* (1−2), 181−186. (b) Sulaeman, U.; Yin, S.; Sato, T. *Appl. Catal., B* **2011**, *105* (1−2), 206−210. (c) Li, H. H.; Yin, S.; Wang, Y. H.; Sekino, T.; Lee, S. W.; Sato, T. *J. Catal.* **2013**, *297*, 65−69. (d) Wang, D. F.; Ye, J. H.; Kako, T.; Kimura, T. *J. Phys. Chem. B* **2006**, *110* (32), 15824−15830. (e) Jia, Y. S.; Shen, S.; Wang, D. G.; Wang, X.; Shi, J. Y.; Zhang, F. X.; Han, H. X.; Li, C. *J. Mater. Chem. A* **2013**, *1* (27), 7905−7912.

(5) Niishiro, R.; Kato, H.; Kudo, A. *Phys. Chem. Chem. Phys.* **2005**, *7* (10), 2241−2245.

(6) Xie, T. H.; Sun, X.; Lin, J. *J. Phys. Chem. C* **2008**, *112* (26), 9753−9759.

(7) Zhou, X.; Shi, J. Y.; Li, C. *J. Phys. Chem. C* **2011**, *115* (16), 8305−8311.

(8) (a) Konta, R.; Ishii, T.; Kato, H.; Kudo, A. *J. Phys. Chem. B* **2004**, *108* (26), 8992−8995. (b) Bae, S. W.; Borse, P. H.; Lee, J. S. *Appl. Phys. Lett.* **2008**, *92* (10), 104107.

(9) Asai, R.; Nemoto, H.; Jia, Q.; Saito, K.; Iwase, A.; Kudo, A. *Chem. Commun.* **2014**, *50* (19), 2543−2546.

(10) (a) Ouyang, S. X.; Tong, H.; Umezawa, N.; Cao, J. Y.; Li, P.; Bi, Y. P.; Zhang, Y. J.; Ye, J. H. *J. Am. Chem. Soc.* **2012**, *134* (4), 1974−1977. (b) Reunchan, P.; Ouyang, S. X.; Umezawa, N.; Xu, H.; Zhang, Y. J.; Ye, J. H. *J. Mater. Chem. A* **2013**, *1* (13), 4221−4227.

(11) Wang, Q.; Hisatomi, T.; Ma, S. S. K.; Li, Y. B.; Domen, K. *Chem. Mater.* **2014**, *26* (14), 4144−4150.

(12) Jia, A. Z.; Liang, X. Q.; Su, Z. Q.; Zhu, T.; Liu, S. X. *J. Hazard. Mater.* **2010**, *178* (1−3), 233−242.

(13) (a) Wang, X. C.; Maeda, K.; Thomas, A.; Takanabe, K.; Xin, G.; Carlsson, J. M.; Domen, K.; Antonietti, M. *Nat. Mater.* **2009**, *8* (1), 76−80. (b) Ikeda, S.; Hara, M.; Kondo, J. N.; Domen, K.; Takahashi, H.; Okubo, T.; Kakihana, M. *Chem. Mater.* **1998**, *10* (1), 72−77. (c) Sayama, K.; Yase, K.; Arakawa, H.; Asakura, K.; Tanaka, A.; Domen, K.; Onishi, T. *J. Photochem. Photobiol., A* **1998**, *114* (2), 125−135. (d) Kudo, A.; Kato, H.; Nakagawa, S. *J. Phys. Chem. B* **2000**, *104* (3), 571−575.

(14) (a) Miseki, Y.; Kato, H.; Kudo, A. *Energy Environ. Sci.* **2009**, *2* (3), 306−314. (b) Jeong, E. D.; Ha, M. G.; Won, M. S.; Kim, H. G.; Pak, H. K.; Borse, P. H.; Ji, S. M.; Lee, J. S. *J. Korean Phys. Soc.* **2006**, *49*, S671−S674. (c) Kim, H. G.; Hwang, D. W.; Kim, J.; Kim, Y. G.; Lee, J. S. *Chem. Commun.* **1999**, *12*, 1077−1078.

(15) (a) Mitchell, R. H. *Perovskites: Modern and Ancient*; Almaz Press Inc.: Ontario, Canada, 2002; p 317. (b) Kim, H. G.; Becker, O. S.; Jang, J. S.; Ji, S. M.; Borse, P. H.; Lee, J. S. *J. Solid State Chem.* **2006**, *179* (4), 1214−1218.

(16) (a) Druce, J.; Ishihara, T.; Kilner, J. *Solid State Ionics* **2014**, *262*, 893−896. (b) Jung, W.; Tuller, H. L. *Energy Environ. Sci.* **2012**, *5* (1), 5370−5378. (c) Lehuta, K. A.; Kittilstved, K. R. *J. Mater. Chem. A* **2014**, *2* (17), 6138−6145.

(17) Nurlaela, E.; Ould-Chikh, S.; Harb, M.; del Gobbo, S.; Aouine, M.; Puzenat, E.; Sautet, P.; Domen, K.; Basset, J. M.; Takanabe, K. *Chem. Mater.* **2014**, *26* (16), 4812−4825.

(18) Larson, A. C.; Von Dreele, R. B. *General Crystal Structure Analysis System (GSAS)*; Los Alamos National Laboratory Report No. LA-UR-86-748; The Regents of the University of California: Oakland, CA, 1994.

(19) Van der Heide, P. *X-ray Photoelectron Spectroscopy: An Introduction to Principles and Practices*; John Wiley & Sons, Inc: Hoboken, NJ, 2012.

(20) Kortum, G.; Braun, W.; Herzog, G. *Angew. Chem., Int. Ed. Engl.* **1963**, *2* (7), 333−341.

(21) (a) Xu, X. X.; Liu, G.; Randorn, C.; Irvine, J. T. S. *Int. J. Hydrogen Energy* **2011**, *36* (21), 13501−13507. (b) Xu, X. X.; Liu, G.; Azad, A. K. *Int. J. Hydrogen Energy* **2015**, *40*, 3672−3678.

(22) Kresse, G.; Furthmuller, J. *Phys. Rev. B: Condens. Matter Mater. Phys.* **1996**, *54* (16), 11169−11186.

(23) Perdew, J. P.; Burke, K.; Ernzerhof, M. *Phys. Rev. Lett.* **1996**, *77* (18), 3865−3868.

(24) Kresse, G.; Joubert, D. *Phys. Rev. B: Condens. Matter Mater. Phys.* **1999**, *59* (3), 1758−1775.

(25) Monkhorst, H. J.; Pack, J. D. *Phys. Rev. B* **1976**, *13* (12), 5188−5192.

(26) Shannon, R. D.; Prewitt, C. T. *Acta Crystallogr., Sect. B: Struct. Crystallogr. Cryst. Chem.* **1969**, *25*, 925−946.

DOI: 10.1021/acs.inorgchem.5b01042
Inorg. Chem. 2015, 54, 7445−7453

(27) Hua, L.; Chan, Y. C.; Wu, Y. P.; Wu, B. Y.; Karabi, S.; Tan, S. C. A highly selective technique to determine hexavalent chrominum in electronic and electrical products for RoHS compliance. In *6th International IEEE Conference on Polymers and Adhesives in Microelectronics and Photonics*; IEEE CPMT Society: Odaiba, Tokyo, Japan, 2007.
(28) (a) Vasquez, R. P. *J. Electron Spectrosc. Relat. Phenom.* **1991**, *56* (3), 217−240. (b) Aika, K.; Aono, K. *J. Chem. Soc., Faraday Trans.* **1991**, *87* (8), 1273−1277.
(29) Takata, T.; Domen, K. *J. Phys. Chem. C* **2009**, *113* (45), 19386−19388.
(30) Phivilay, S. P.; Puretzky, A. A.; Domen, K.; Wachs, I. E. *ACS Catal.* **2013**, 3 (12), 2920−2929.
(31) Xiao, H.; Tahir-Kheli, J.; Goddard, W. A. *J. Phys. Chem. Lett.* **2011**, *2* (3), 212−217.
(32) Cox, P. A. *The Electronic Structure and Chemistry of Solids*; Oxford University Press: Oxford, U.K., 1987.
(33) (a) Kittel, C. *Introduction to Solid State Physics*, 7th ed.; Wiley: New York, 1996. (b) Mizoguchi, H.; Woodward, P. M. *Chem. Mater.* **2004**, *16* (25), 5233−5248.

DOI: 10.1021/acs.inorgchem.5b01042
Inorg. Chem. 2015, 54, 7445−7453